
COUNTERFACTUAL EXPERIENCE AUGMENTED OFF-POLICY REINFORCEMENT LEARNING

Sunbowen Lee,* Yicheng Gong[†]
Hubei Province Key Laboratory of
System Science in Metallurgical Process
College of Science
Wuhan University of Science and Technology
Wuhan, China
{bw1863, gongyicheng}@wust.edu.cn

Chao Deng
Intelligent Automobile Engineering Research Institute
School of Automobile and Traffic Engineering
Wuhan University of Science and Technology
Wuhan, China
woec@wust.edu.cn

ABSTRACT

Reinforcement learning control algorithms face significant challenges due to out-of-distribution and inefficient exploration problems. While model-based reinforcement learning enhances the agent’s reasoning and planning capabilities by constructing virtual environments, training such virtual environments can be very complex. In order to build an efficient inference model and enhance the representativeness of learning data, we propose the Counterfactual Experience Augmentation (CEA) algorithm. CEA leverages variational autoencoders to model the dynamic patterns of state transitions and introduces randomness to model non-stationarity. This approach focuses on expanding the learning data in the experience pool through counterfactual inference and performs exceptionally well in environments that follow the bisimulation assumption. Environments with bisimulation properties are usually represented by discrete observation and action spaces, we propose a sampling method based on maximum kernel density estimation entropy to extend CEA to various environments. By providing reward signals for counterfactual state transitions based on real information, CEA constructs a complete counterfactual experience to alleviate the out-of-distribution problem of the learning data, and outperforms general SOTA algorithms in environments with difference properties. Finally, we discuss the similarities, differences and properties of generated counterfactual experiences and real experiences. The code is available at <https://github.com/Aegis1863/CEA>.

Keywords Reinforcement learning · Variational autoencoder · Counterfactual inference · Bisimulation

1 Introduction

Advanced control strategies have attracted substantial interest, particularly with recent progress in deep learning and reinforcement learning (RL). But all learning-based algorithms face the out-of-distribution (OOD) problem. In the field of online RL, data must be collected from the environment in real time without domain knowledge, making it very difficult for RL agents to learn comprehensive policies in underrepresented state distributions.

There are many attempts to solve the OOD problem. For example, RAD [1], DBC [2], DrAC [3], DrQ [4, 5], SODA [6], etc., these methods effectively make use of representation learning and data enhancement methods. They transfer the image enhancement method in computer vision to vision-based RL, achieving a robust and efficient control effect. They are usually applied to robot control, but not for tasks with vector-based observation. Specifically, most of them enhance the robustness of convolutional parameters by rotating or adding noise to the observed images. However, for a dense vector, these methods will destroy its information. The data enhancement of dense vectors requires a more conservative and cautious approach. We noticed a related work based on vector observation augmentation, Acamda [7], but there is no code, and it is difficult to reproduce. Therefore, we provide an executable method with open-source code.

*First author

[†]Corresponding author

To effectively handle dense vectors, autoencoders have been regarded as effective tools. For example, sequential encoders [8, 9, 10] are implemented for future estimation. Generally, autoencoders have the ability to compress and reconstruct features. Among them, the conditional variational autoencoder (CVAE) [11, 12] can generate corresponding feature vectors or matrices based on different conditions. **Therefore, our first motivation lies in using CVAE to generate transfer vectors that have both randomness and directionality, as a supplement to the original state transition data.** We construct a state transition autoencoder (STA) based on CVAE for inference.

STA solves the reasoning problem, but we need conditions to perform reasoning. Here, the conditions should be actions that have not occurred, also known as counterfactual actions. And, the counterfactual action will produce a counterfactual result, this process is called counterfactual (or virtual) state transition. Generally speaking, actions that have already occurred are known, but there may be a very large number of actions that have not occurred and are difficult to traverse. **In this case, our second motivation lies in achieving efficient and resource-saving counterfactual action sampling.** Simply put, we construct a Gaussian kernel density estimation function in the action space and determine representative counterfactual actions through the method of maximum entropy sampling.

Traditionally, building a model to fit the environment is a good way to predict future states and reward values, as implementation by Janner et al. [13], but we found that in many environments, the prediction error of reward values is very large. **Thus, our third motivation is to reduce this error, by matching the real reward values to counterfactual state transitions.** After that, we can construct complete counterfactual experiences. Additionally, this matching method is based on the assumption of bisimulation, which will be introduced in Section 3.

In short, by integrating the methods proposed previously, we use the counterfactual actions obtained from sampling as conditions, enabling the STA inference to obtain possible counterfactual results. We then compare the counterfactual result with real data, pairing the closest data through the minimum Euclidean distance and assigning the true reward value to the counterfactual result. Our concept of counterfactual is consistent with Pearl’s work [14]. We present an explanatory diagram of counterfactual reasoning learning in Fig. 1.

In summary, this paper introduces the STA, and counterfactual experience augmentation (CEA) algorithm. The code is available in <https://github.com/Aegis1863/CEA>.

Our main contributions are as follows:

1. We introduce the STA, a model that learns state transition dynamics with inherent randomness, enabling counterfactual reasoning capabilities.
2. We design a maximum entropy sampling optimization method based on Gaussian kernel density estimation for counterfactual action sampling.
3. We propose a comprehensive CEA algorithm, which uses counterfactual action sampling and STA model for counterfactual reasoning to alleviate the OOD problem of learning data and can effectively improve the performance of the backbone model.

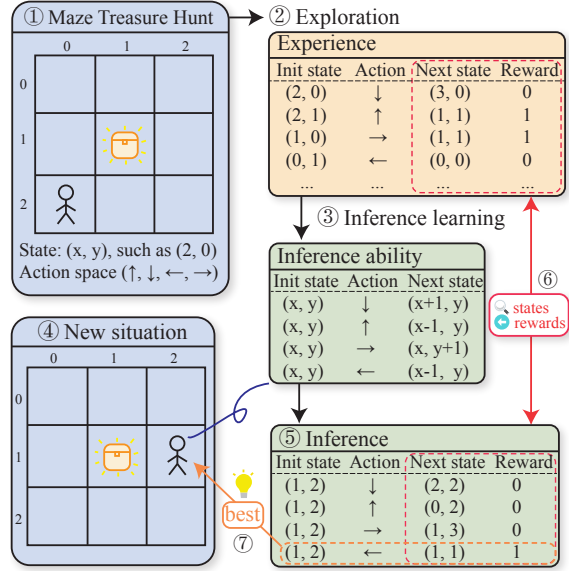


Figure 1: Counterfactual inference learning. The agent’s task is to find the treasure chest. When the agent moves to a state with the same coordinate as the treasure chest, the reward increases by 1, otherwise remains 0. We marked the entire process with serial numbers in the figure. In the first and second steps, the agent randomly selects its action and records the process of position transfer. This record can be used for inference learning, with its ability referring to table "Inference ability". Once this inference ability is obtained, it can be used to infer the results of the corresponding actions in new situations like step four. The agent can compare the predicted results with historical information, as shown in step six, thereby choosing the best action without actually executing the action. The action space and state space of the environment are both discrete, which satisfies the bisimulation assumption.

In the following text, Section 2 introduces related work, while Section 3 introduces basic methods. Our implementation is in Section 4, which also includes some experimental demonstrations. Section 5 introduces the testing environment and comparison algorithms. We present the experimental results and analysis in Section 6, and provide the details of the innovation points in Section 7. Finally, we give our discussion and conclusion in Section 8 and 9.

2 Related works

Our work belongs to model-based RL. We also utilize the theory of causal inference and bisimulation as the basis for data augmentation. Therefore, this section presents this existing research.

2.1 Deep RL

Q-learning [15], a fundamental off-policy technique, estimates cumulative rewards for state-action pairs without requiring an environment model. The introduction of Deep Q Networks (DQN) [16] enhanced this approach by using convolutional neural networks to approximate Q-values, incorporating experience replay and target networks for improved stability. Deep Deterministic Policy Gradient (DDPG) [17] extends these principles to continuous action spaces, using an actor-critic architecture with off-policy learning. Soft Actor-Critic (SAC) [18, 19] further improves this framework by adding entropy regularization to balance exploration and exploitation. Experience management, through techniques like prioritized experience replay (PER) [20], improves data efficiency by prioritizing valuable experiences. At the same time, some multi-agent solutions based on Deep RL have gradually been proposed [21, 22, 23].

2.2 Model-based and causal RL

Model-based RL leverages environment models to enhance decision-making. The probabilistic ensemble trajectory sampling algorithm [24] uses a probabilistic model to handle uncertainty, while other similar methods [25, 13, 8] also show strong performance.

Causal RL, which integrates causal inference into learning, is an emerging field. Yang et al. [26] introduced a causal factor for agents in multi-agent tasks, while Sun et al. [7] used adversarial models to augment experiences, though both lacked clear solutions for reward signals in counterfactual state transitions. Chao et al. [27] proposed using structural causal models for state dynamics, providing a more detailed theoretical approach. We noticed that Pitis et al. [28] proposed a model-based causal RL method, MoCoDa, which is combined with data augmentation.

2.3 Data augmentation RL

As mentioned in the introduction, many data augmentation RL serves tasks with observation data as images, because it is easy to draw on the experience of computer vision. They have some methods to supplement data using cropping, rotation, and noise, such as RAD [1], DrQ [4]. While CURL [29], DBC [2] and SODA [6] improve the model recognition ability through contrastive learning. We discovered a new data augmentation method based on vector observations, namely Acamda [7] proposed by Sun et al. Acamda proposes to use bidirectional conditional causal generative adversarial network for reasoning, which is similar to ours. Unfortunately, this method can hardly be reproduced. We provide a horizontal comparison of these peer works in Table 1.

Next, we will introduce the preliminary theory and method of our work.

3 Preliminary

This section introduces preliminary methods, which are the foundation of our model.

3.1 Reinforcement learning

RL are usually defined in Markov decision processes (MDP), as detailed by Sutton et al. [30, 31, 32]. We assume that the underlying environment is a MDP, characterized by the tuple $\mathcal{M} = (\mathcal{S}, \mathcal{A}, \mathcal{P}, \mathcal{R}, \gamma)$. In this framework, \mathcal{S} denotes the set of states, \mathcal{A} represents the set of actions, $\mathcal{P}(s'|s, a)$ specifies the probability of transitioning from state $s \in \mathcal{S}$ to state $s' \in \mathcal{S}$, and $\gamma \in [0, 1)$ is a discount factor that determines the importance of future rewards. An agent chooses actions $a \in \mathcal{A}$ according to a policy $a \sim \pi(s)$, which then influences the next state $s' \sim \mathcal{P}(s, a)$ and generates a reward $r = \mathcal{R}(s) \in \mathbb{R}$. The agent’s goal is to find a policy that maximizes the expected sum of discounted rewards over time: $\max_{\pi} \mathbb{E}_{\mathcal{P}}[\sum_{t=0}^{\infty} \gamma^t \mathcal{R}(s_t)]$. The current general deep RL SOTA algorithms all serve the goal of maximizing the final reward, and the main method includes temporal difference and policy gradient.

Table 1: Comparison of data augmentation RL. In the table, Causal indicates whether the method involves a causal framework, Domain represents the observed form to be addressed. Model denotes whether the method is model-based. Year corresponds to their proposed time. Code indicates whether the method has open-source code.

Algorithm	Causal	Domain	Model	Year	Code
MBPO [13]	no	any	yes	2019	yes
RAD [1]	no	pixel	no	2020	yes
CURL [29]	no	pixel	no	2020	yes
DrAC [3]	no	pixel	no	2020	yes
DrQ [4]	no	pixel	no	2021	yes
SODA [6]	no	pixel	no	2021	yes
MoCoDa [28]	yes	pixel	yes	2022	yes
Acamda [7]	yes	vector	yes	2024	no
CEA (Ours)	yes	vector	yes	2024	yes

CEA are built on DQN and DDPG, which have become important application methods of temporal difference. We will give a brief introduction below.

Considering that the timing difference error is usually expressed as:

$$\delta_t = r_t + \gamma \cdot \max_{a'} Q(s_{t+1}, a') - Q(s_t, a_t). \quad (1)$$

The parameters of the DQN are updated as

$$\omega' = \operatorname{argmin}_{\omega} \frac{1}{2N} \sum_{i=1}^N \left[Q_{\omega}(s_t^i, a_t^i) - (r_t^i + \gamma Q_{\omega}(s_{t+1}^i, \operatorname{argmax}_a Q_{\omega}(s_{t+1}^i, a))) \right]^2, \quad (2)$$

where ω is network parameters; Q_{ω} is the Q function; s_t^i , a_t^i , r_t^i and s_{t+1}^i respectively stand for the state, action, reward and next state in time step t or $t + 1$; N is the number of samples. While γ is the discount factor.

In the neural network model, we modify the structure to have a dueling form. The optimal target is defined as:

$$Q_{\lambda, \alpha, \beta}(s, a) = V_{\lambda, \alpha}(s) + A_{\lambda, \beta}(s, a) - \frac{1}{|A|} \sum_{a'} A_{\lambda, \beta}(s, a'), \quad (3)$$

where $V_{\lambda, \alpha}(s)$ is the state value function, $A_{\lambda, \beta}(s, a)$ is the advantage function. λ represents the sharing parameters of V and A function. α and β are the private parameters of V and A function respectively. The purpose of subtracting the average value from the advantage function is to guide the network to update the value function V . Otherwise, the network may be inclined to make $V = 0$ and A degenerate to Q . On the other hand, calculating the difference between A and its average value is also to allow the neural network to learn the value difference between various actions.

DQN can usually only cope with discrete action decision tasks. In order to extend the value learning method to the continuous action space, DDPG constructs two networks, one serving as the actor and the other as the critic. The actor network is based on a policy function and directly outputs a deterministic action for a given state, which differentiates it from traditional value-based methods that output a probability distribution over actions. The critic network, on the other hand, is based on the Q -value function and evaluates the value of a given state-action pair. In DDPG, the actor network relies on the critic network to optimize its policy. Specifically, the critic network learns the Q -values by minimizing the temporal difference error, while the actor network updates its policy by maximizing the Q -values provided by the critic network. This combination of policy gradient methods and value-based methods allows DDPG to efficiently learn policies in continuous action spaces.

In simple terms, the update formula of Q function can be expressed as:

$$Q(s_t, a_t) \leftarrow r_t + \gamma \max_{a^*} Q(s_{t+1}, a^*). \quad (4)$$

In off-policy, a batch of experiences is usually extracted from the experience pool as a small batch. Each experience consists of a tuple $\{s, a, s', r\}$, and the Q value is estimated by the mean calculation method:

$$Q(s, a) \approx \frac{1}{N} \sum_{i=1}^N r_i + \gamma \max_{a^*} Q(s'_i, a^*), \quad (5)$$

where s' is the random variable form of s_{t+1} . Therefore, increasing N is conducive to accurately estimating the Q function and reducing the estimation variance:

$$\text{Var}(\hat{Q}) \propto \frac{\sigma^2}{N}, \quad (6)$$

and this is equivalent to alleviating the OOD of state distribution.

Based on traditional off-policy algorithm, PER takes into account the importance of experience.

3.2 Prioritized experience replay

PER assigns an importance value to each experience, which is directly proportional to the temporal difference error as computed by Equation 1. The higher the error, the greater the assigned importance. The importance weight update process is governed by:

$$P_i = \frac{\omega_i^\delta}{\sum_k \omega_k^\delta}, \quad (7)$$

$$w_i = \left(\frac{1}{N} \cdot \frac{1}{P_i} \right)^\eta,$$

where δ determines the priority level, and it degrades to uniform sampling when η is 0. The size of experience pool is denoted by N . η stands for a parameter controlling the weight magnitude, typically increases gradually during the training process. We consider PER to manage numerous experiences and ensure that low-value samples are underestimated. However, PER may not always help, which will be used as an ablation condition in the experiments.

We next introduce the concept of counterfactual inference.

3.3 Counterfactual inference

cmGiving Fig. 2 as directed acyclic causal graph, s_i and s_j are two different states, a_i and a_j are two corresponding actions. Different state-action pairs may lead to the same or similar state transition result s and the same reward r . This is consistent with the bisimulation property mentioned in the previous part.

In the figure, s_i and a_i affect the intermediate state s , and s further affects the reward r . s can be regarded as the mediating variable of s_i and a_i on r . This constitutes a case of the front door effect. The same is true for s_j and a_j . Therefore, s can be used to analyze the causal effect of different action states on the final reward r . For example, we consider randomly sampling some s dividing into two groups, s_i and s_j , and find the a_i corresponding to s_i . Then sampling some not occurred \hat{a}_j by maximum entropy method, and using the autoencoder to generate s . \hat{a}_j represents a counterfactual action that the agent has not yet practiced.

Next, we present the bisimulation property and why we emphasize this point.

3.4 Bisimulation

We use bisimulation as a theoretical basis because obviously no model can predict the future accurately, but in some cases, it can be approximated, which depends on the bisimulation property. At the same time, we also need to point out that not all tasks meet this condition. We will define bisimulation based on the definition of MDP in Subsection 3.1. Bisimulation is a form of state abstraction that groups states s_i and s_j that are "behavioral equivalent" [33].

For a standard definition [34]: an equivalence relation B between states is a bisimulation relation if, for all states $s_i, s_j \in \mathcal{S}$, that are equivalent under B (denoted $s_i \equiv_B s_j$) the following conditions hold:

$$\begin{aligned} \mathcal{R}(s_i, \mathbf{a}) &= \mathcal{R}(s_j, \mathbf{a}) \quad \forall \mathbf{a} \in \mathcal{A}, \\ \mathcal{P}(G | s_i, \mathbf{a}) &= \mathcal{P}(G | s_j, \mathbf{a}) \quad \forall \mathbf{a} \in \mathcal{A}, \forall G \in \mathcal{S}_B, \end{aligned} \quad (8)$$

where \mathcal{S}_B is the partition of \mathcal{S} under the relation B (the set of all groups G of equivalent states), and $\mathcal{P}(G | s, \mathbf{a}) = \sum_{s' \in G} \mathcal{P}(s' | s, \mathbf{a})$.

In short, for two different states, if the actions they take lead to the same state transition results, they can be regarded as satisfying the bisimulation property. However, in the continuous state space, it is almost impossible for

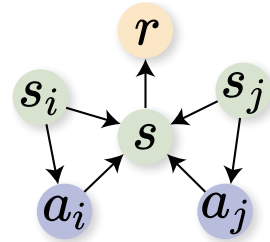


Figure 2: Causal directed acyclic graph of state transition process. In this case, different state-action pairs will lead to the same result, satisfying the bisimulation property.

two states to be exactly the same, so we regard the case of similar state distribution as approximately satisfying the bisimulation property.

In our work, if the result of state transfer in virtual experience is the same as the result of a real state transfer, then we think their state transfer reward is the same.

The maximum entropy sampling, STA and other important implementations will be introduced in the next section.

4 Methodology

This section introduces all implementations of our work.

4.1 State transition autoencoder

RL based on generative models has made great progress, such as diffusion RL and generative adversarial RL [35, 36, 37]. This paper presents a simple and practical method based on a CVAE.

In order to make the model focus on more significant characteristics, STA learns the difference between state transitions and represented by d . Let d as an input and d' is a generated output. d is calculated as:

$$d_t = s_{t+1} - s_t, \quad (9)$$

where s_{t+1} and s_t are next and current state, respectively. The way to get the agent to learn state transitions is a classic application in [38] and [13], which emphasizes understanding the underlying transition process, making it more amenable to learning.

To incorporate the counterfactual action \hat{a} as conditions in the latent variable, the process differs depending on the type of action space. In discrete action space, the actions are countable, all actions other than those that have been performed are counterfactuals. For continuous action spaces, sampling is required, and the number of samples for \hat{a} should be manually adjusted. Counterfactual action sampling in continuous action space will be introduced in the next subsection

Consequently, STA follows the structure of CVAE, focusing on the dynamics of state transitions. By introducing a latent variable z , we can compute the probability density function of d conditioned on a through the construction of marginal likelihood:

$$\log p(d|a) = \log \int p(d|z, a)p(z|a)dz. \quad (10)$$

We introduce the variational distribution $q(z|d, a)$ as an approximate representation, aiming to capture the underlying structure of the latent variables z given the observed data d and condition a . It should be noted that we hope that $p(z|a)$ conforms to the standard Gaussian distribution, which is convenient for calculation and sampling.

According to Jensen’s inequality, we can derive evidence lower bound:

$$\begin{aligned} \log p(d|a) &\geq \mathbb{E}_{q(z|d, a)} \left[\log \frac{p(d|z, a)p(z|a)}{q(z|d, a)} \right] \\ &= \mathbb{E}_{q(z|d, a)} [\log p(d|z, a)] - \\ &\quad \mathbb{D}_{KL} [q(z|d, a) || p(z|a)], \end{aligned} \quad (11)$$

where the objective involves a reconstruction loss term $\mathbb{E}_{q(z|d, a)} [\log p(d|z, a)]$, which measures the discrepancy between the generated and real data. While \mathbb{D}_{KL} is the Kullback-Leibler divergence, which quantifies the difference between the approximate distribution $q(z|d, a)$ and the prior distribution $p(z|a)$.

We mentioned that $p(z|a)$ is a standard Gaussian distribution, and $q(z|d, a)$ also follows a Gaussian distribution, but its mean μ and variance σ^2 are determined by an encoder model (a neural network). At this time, $\mathbb{D}_{KL} [q(z|d, a) || p(z|a)]$ is calculable, that is

$$\mathcal{L}_{kl} = \frac{1}{2} \sum_{i=1}^n [\mu_i^2 + \sigma_i^2 - \log \sigma_i^2 - 1], \quad (12)$$

where i refers to the i th sample. We refer to the proof of Su [39] for details provided in Appendix A.

The reconstruction error $\mathbb{E}_{q(z|d, a)} [\log p(d|z, a)]$, computed as the mean squared error, is the difference between the reconstructed data d'_i and the original data d_i , and is given as:

$$\mathcal{L}_r = \frac{1}{2n} \sum_{i=1}^n (d'_i - d_i)^2. \quad (13)$$

Therefore, the optimization goal of STA is to minimize the total loss:

$$\mathcal{L} = \mathcal{L}_r + \mathcal{L}_{kl}. \quad (14)$$

By minimizing the loss, generated d' is optimized to closely approximate d . With the use of STA, we proceed by sampling a vector z' from a Gaussian distribution, concatenating it with counterfactual actions and forwarding it to the decoder. This process generates a transition vector d' . Subsequently, we create a counterfactual next state by adding d' to the current state s . The next challenge lies in providing an appropriate virtual reward signal, which we will address in the subsequent subsection.

4.2 Counterfactual action sampling

cmAction sampling actions from discrete action spaces are easy, the method used in this paper is to reason about all unsampled action choices as counterfactual actions. Therefore, this section introduces how to extend CEA to the counterfactual action sampling method in continuous action spaces. This approach can be applied to discrete action spaces as well.

In continuous action spaces, the sampling is troublesome. This paper proposes to construct a probability density based on existing data through Gaussian kernel density estimation, then randomly initialize some samples. These randomly initialized samples are the counterfactual action samples to be optimized.

The reason for choosing the Gaussian kernel function is that it has no parameter and has an explicit expression. At this point, we can focus only on optimizing the input variables without having to tune the model. While the explicit expression makes the optimization target formula differentiable, so that the approximate solution can be obtained by the gradient descent. Another benefit is that the Gaussian kernel gives smoother estimates and can more easily handle data with long-tailed distributions, which aligns our data characteristics.

The optimization of these counterfactual samples should maximize the entropy of the new kernel density. **In other words, we hope that counterfactual samples can be fully distributed in those desolate spaces.** The following is the specific sampling method.

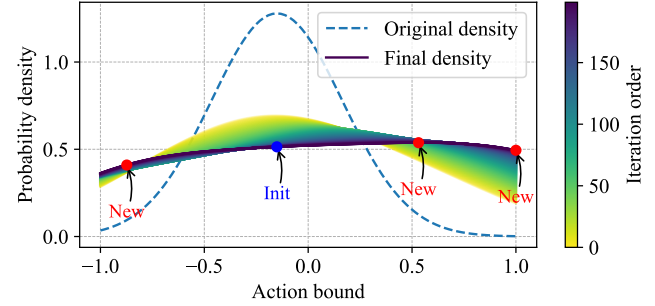
We initialize some counterfactual actions \hat{a} and merge it with the known samples a to get a new action set A . While it is theoretically possible to have multiple a , in practice there is only one, because we will deal with each experience sample separately, with only one a in each experience.

Our goal is

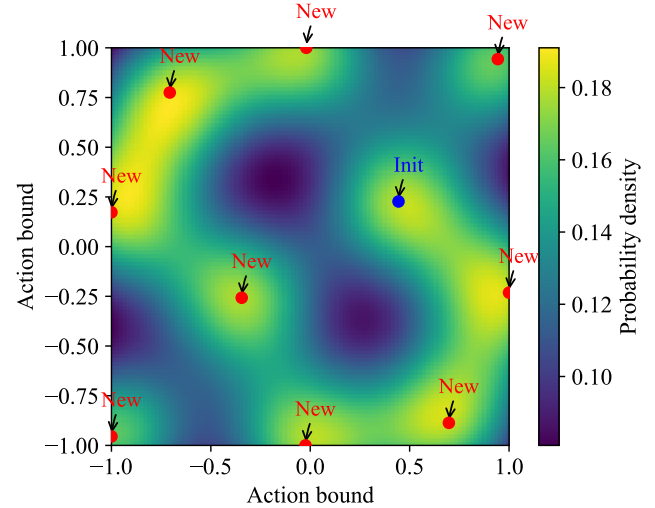
$$\max_{\{\hat{a}_1, \hat{a}_2, \dots, \hat{a}_n\}} - \sum_{x \in A} p(x) \log p(x). \quad (15)$$

We implement gradient descent method for numerical optimization. Let $y(x) = p(x) \log p(x)$ and be shortened to y . Split the domain into m parts and use trapezoidal integration to approximate the entropy:

$$\begin{aligned} H(x) &= - \int p(x) \log p(x) dx \\ &\approx - \sum_{j=1}^{m-1} \left(\frac{x_j - x_{j-1}}{2} \right) (y_j + y_{j-1}). \end{aligned} \quad (16)$$



(a) Sampling in 1-dimensional action space. Three new samples that can be optimized are set for one initial sample.



(b) Sampling in 2-dimensional action space. Nine new samples that can be optimized are set for one initial sample.

Figure 3: Sampling based on kernel density estimation

According to the Gaussian kernel density estimation, for p , we have

$$p(x) = \frac{1}{|A|h\sqrt{2\pi}} \sum_{i=1}^{|A|} \exp \left\{ -\frac{(x - a_i)^2}{2h^2} \right\}, \quad (17)$$

where $|A|$ represents the length of the set \hat{A} . The gradient of H w.r.t \hat{a} is

$$\frac{\partial H}{\partial \hat{a}} = - \sum_{j=1}^{m-1} \left(\frac{x_j - x_{j-1}}{2} \right) \left(\frac{\partial y_j}{\partial \hat{a}} + \frac{\partial y_{j-1}}{\partial \hat{a}} \right). \quad (18)$$

Since the value of j depends on m , we remove the subscript and consider the expression of y alone:

$$\begin{aligned} y(x) &= p(x) \log p(x), \\ \log p(x) &= -\log(|A|h\sqrt{2\pi}) + \sum_{i=1}^{|A|} \left[-\frac{(x - a_i)^2}{2h^2} \right], \\ \frac{\partial y}{\partial \hat{a}} &= \frac{\partial p(x)}{\partial \hat{a}} [\log p(x) + 1], \end{aligned} \quad (19)$$

where

$$\begin{aligned} \frac{\partial p(x)}{\partial \hat{a}} &= -\frac{1}{|A|h\sqrt{2\pi}} \exp \left\{ -\frac{(x - \hat{a})^2}{2h^2} \right\} \cdot \frac{x - \hat{a}}{h^2} \\ &= -\frac{x - \hat{a}}{|A|h^3\sqrt{2\pi}} \exp \left\{ -\frac{(x - \hat{a})^2}{2h^2} \right\}. \end{aligned} \quad (20)$$

Therefore, the differential of y w.r.t \hat{a} can be found as

$$\begin{aligned} \frac{\partial y}{\partial \hat{a}} &= \frac{\partial p(x)}{\partial \hat{a}} [\log p(x) + 1] \\ &= -\frac{x - \hat{a}}{|A|h^3\sqrt{2\pi}} \exp \left\{ -\frac{(x - \hat{a})^2}{2h^2} \right\} \cdot \\ &\quad \left\{ -\log(|A|h\sqrt{2\pi}) + \sum_{i=1}^{|A|} \left[-\frac{(x - a_i)^2}{2h^2} \right] + 1 \right\}. \end{aligned} \quad (21)$$

The calculation of $\frac{\partial y_j}{\partial \hat{a}}$ and $\frac{\partial y_{j-1}}{\partial \hat{a}}$ is similar. We can substitute them into Equation 18 to calculate the specific gradient. In summary, the gradient of the initial sampling action based on maximizing information entropy is calculable. Once the gradient value is calculated, it can be multiplied by a learning rate and added to the original values of \hat{a} for multiple iterations, as shown in Equation 22. Therefore, those samples can be optimized.

$$\hat{a} \leftarrow \hat{a} + lr \cdot \frac{\partial H}{\partial \hat{a}}. \quad (22)$$

In this case, Equation. 15 is solvable, therefore, here we provide the expression for obtaining the counterfactual action \hat{a}_i :

$$\{\hat{a}_1, \hat{a}_2, \dots, \hat{a}_n\} = \underset{\hat{a}_1, \hat{a}_2, \dots, \hat{a}_n}{\operatorname{argmax}} - \sum_{x \in A} p(x) \log p(x), \quad (23)$$

where the set A include both a real action a and several counterfactual actions $\hat{a}_1, \hat{a}_2, \dots, \hat{a}_n$. We only optimize those counterfactual actions.

Fig. 3(a) and Fig. 3(b) are the sampling experimental results of this method in one-dimensional and two-dimensional data. A known sample is marked with *Init*, and newly added points are marked with *New*. The initial positions of *New* are randomly, and its final position is the result of iterative optimization. It can be observed that the final positions of *New* are evenly distributed in areas where there were originally no samples.

Next, we introduce how to construct a complete counterfactual experience.

4.3 Closest transition pair

Here, we will present the framework of CEA. We commence by constructing an MDP to elucidate the concept of counterfactual actions, followed by detailing the algorithmic procedure of CEA.

Fig. 4 illustrates a MDP example with both a real track and counterfactual actions, and fully satisfies the bisimulation property. Assuming action space is discrete with 3 action options, as shown by the arrows in Fig. 4. This track consists of 7 stages from A to F, with 3 discrete action options per stage. The solid arrows represent real actions, leading to the next state, while dashed arrows symbolize counterfactual actions. At state E, the agent chooses to transfer to F. Using STA, we can infer transition vectors conditioned on hypothetical actions, allowing us to compute an estimated next state. If, for instance, E could hypothetically reach B through a counterfactual action, we term $\{A, B\}$ and $\{E, B\}$ as closest transition pair (CTP). Therefore, as long as the next state transferred to is consistent or similar, a CTP can be formed. Since $\{A, B\}$ is a factual history with complete information, we assign the reward of $\{A, B\}$ to $\{E, B\}$. In simple terms, the implementation of CTP can be expressed as finding index i^* of samples:

$$\begin{aligned} r^* &= r_{i^*}, \\ i^* &= \arg \min_i d(\hat{s}_i, s), \end{aligned} \quad (24)$$

where \hat{s} is the counterfactual next state calculated by STA, and s is the real state that already exists in the experience pool. The distance function d can use Euclidean distance or Manhattan distance.

This shows the result orientation of bisimulation. We give a direct example, with the abuse of symbols, which are only used here. Assume that we known state transition pairs such as $\{s_t^r, a_t^r, s_{t+1}^r, r\}$, which represent the state and action in time step t , and the next state and reward of this state transition. Meanwhile, we give a counterfactual state transition pair $\{s_t^c, a_t^c, s_{t+1}^c\}$ (It currently lacks r). If the transition results s_{t+1} of the two are very close, that is, $s_{t+1}^r \approx s_{t+1}^c$, then we believe that the reward values of the two state transition pairs are consistent. At this time, we copy r in $\{s_t^r, a_t^r, s_{t+1}^r, r\}$ to $\{s_t^c, a_t^c, s_{t+1}^c\}$. Then, we construct a complete counterfactual experience $\{s_t^c, a_t^c, s_{t+1}^c, r\}$.

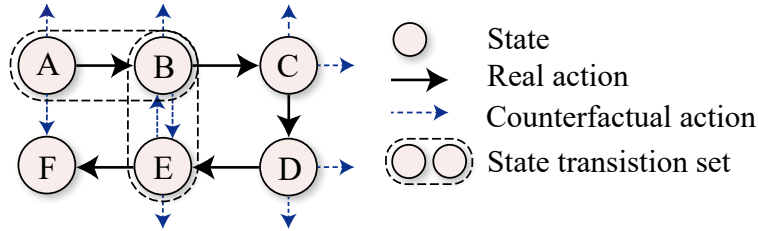


Figure 4: MDP with counterfactual actions

4.4 Counterfactual experience augmentation

cmSince the counterfactual next state cannot be completely consistent with the real state when the state is in continuous spaces, we measure the distance and only consider those state groups with close distance as a CTP. At the same time, the randomness of the autoencoder also helps to simulate the possible non-stationarity of the environment.

As outlined in Algorithm 1, it should be noted that STA needs to be trained in advance, and its training data only needs to be randomly collected from an environment. We compute and sort the difference between the counterfactual next state and the real next state. A threshold ratio can be given as a hyperparameter to filter out those most similar pairs and share the real reward with the counterfactual one. The ratio can also be changed to a specific distance, but it increases the difficulty of fine-tuning. The algorithm framework diagram is shown in Fig. 5.

By incorporating rewards into counterfactual experiences, these expanded experiences are added to the experience pool and sampled alongside real ones. The significance of

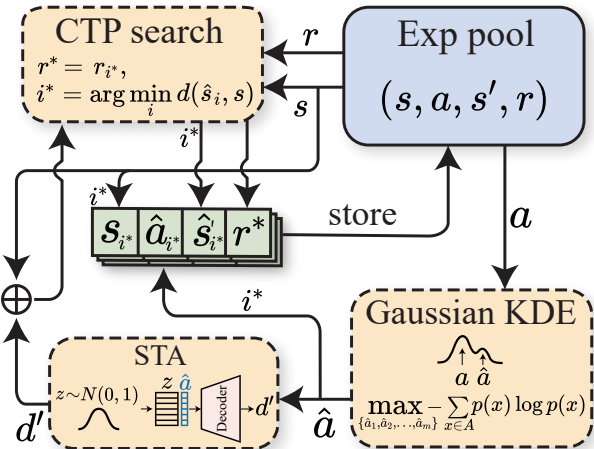


Figure 5: CEA framework

PER lies in managing the large number of potential counterfactual experiences, as with a discrete action space of m and n real experience samples, there can be $n(m - 1)$ counterfactual transitions, leading to rapid expansion of experience. While the similar situation occurs in the continuous action space.

CEA is typically employed in off-policy learning, which is performed before the agent samples the experience. CEA is not supposed to execute frequently. Otherwise, there will be a lot of redundant and similar counterfactual experiences.

It should be noted that the CEA method is built on the basis of Rainbow DQN (RDQN) and DDPG, which are the backbones corresponding to discrete action space tasks and continuous action space tasks respectively. After introducing our methods, the next section gives experimental indicators, details and scenarios.

Algorithm 1 Counterfactual experience augmentation

- 1: **Input:** replay buffer, STA
 - 2: **Output:** Augmented replay buffer
 - 3: Randomly sampling **unsampled** real experience (s, a, r, s') from replay buffer
 - 4: Sampling counterfactual actions \hat{a} from Equation. 23
 - 5: Calculate counterfactual state transition vectors d by giving \hat{a} to STA from $p(d|z, a)$ mentioned in Equation. 10
 - 6: Repeat each state times to create $expand_s$ to align the number of counterfactual data
 - 7: Compute estimated next states: $\hat{s}' = expand_s + d$
 - 8: Retrieve **real** experiences from replay buffer as $(all_s, all_a, all_r, all_ns)$
 - 9: Compute distances between all_ns and \hat{s}' from Equation. 24 and pair the closest top parts and share the real reward r^* to the virtual one
 - 10: Combine $(expand_s, \hat{a}, \hat{s}', r^*)$ as counterfactual experiences
 - 11: Store counterfactual experiences in replay buffer
 - 12: **return** replay buffer
-

5 Experiment settings

We introduce both discrete and continuous action space experimental environments. They are all based on the standard environment wrapped by gymnasium [40].

For discrete action space environments, we use SUMO and Highway, both of which are challenging traffic simulation environments. And they have relatively suitable bisimulation properties. The former is a professional open-source traffic simulation system, and the latter is a simplified driving decision environment. Due to the rapid changes in traffic environments, they are inherently non-stationary [41, 42].

For the continuous action space environments, we use the standard benchmarks Pendulum and Lunar lander (continuous control). They participated in almost all RL algorithm benchmarks. Specific task content and environmental parameters refer to their official documentation [40].

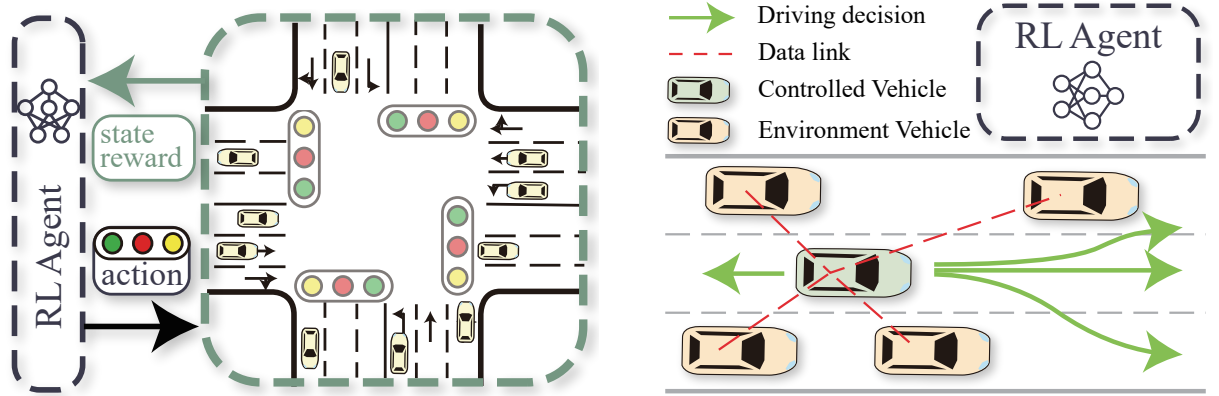
For SUMO and Highway, since they are not widely used simulation benchmarks in the field of RL algorithms, we will give a brief introduction.

5.1 SUMO

SUMO, an established professional traffic simulation system [43], is a popular choice in the traffic simulation research community [44, 45, 46]. We believe that improvements here will be of significant help and inspiration to the field. We employ SUMO as one of our benchmark environment for traffic signal control, as depicted in Fig. 6(a). The goal of the algorithm is to control traffic signals to avoid congestion at the intersection. Given the discrete nature of traffic signal phases, the action space is finite. We analyze the training and control performance of various algorithms using the total reward to evaluate the effectiveness of their training. Total reward is called return as well. Reward in each step is defined as:

$$r_t = w_{t+1} - w_t, \quad (25)$$

where w_{t+1} is sum of waiting times of all vehicles at intersection at time $t + 1$, and the same is true for w_t . Therefore, this reward encourages a smaller difference in the total waiting time at current and previous time points. In fact, other reward signals such as the number of vehicles in queue can also be used, because the fewer vehicles in the queue, the stronger the algorithm’s ability to optimize traffic, but experiments show that the reward signal defined in Equation 25 performs best. The state design follows the design of Alegre et al. [41], which mainly includes lane density, queue vehicle density, etc.



(a) SUMO traffic light control. An Agent will make decisions for a traffic light at an intersection, and the higher the number of waiting vehicles at the intersection, the higher the reward. Its actions are a finite combination of traffic light configurations.

(b) Highway driving decision. Cars are driving on the expressway. The green car, as an agent, needs to make lane-changing decisions. The higher the reward will be when collisions are minimized and the speed is as fast as possible. Its action space size is 4, which are acceleration, deceleration, left turn, or right turn.

Figure 6: Discrete action space benchmark, SUMO and Highway

5.2 Highway

Highway [47] is a simplified road environment, including various scenarios like highways, roundabouts, ramps, etc. It has many lane-changing studies [48, 49] and has become a new test benchmark in the fields of general and transportation. The difference from SUMO is that the control subject is the vehicle instead of the traffic light. Schematic diagram of the two tasks refer to Fig. 6(b). It simulates a small car on a multi-lane highway. Other vehicles on the road are randomly generated, so the control goal of the algorithm is driving decisions, such as which direction to avoid, overtake or slow down. The action space is discrete and simplified to four options: accelerate, slow down, left turn, and right turn.

A controlled vehicle can observe its own and four near vehicles. The observation vector of each vehicle, includes the position, speed and other information in the environment. The reward function is defined as:

$$r_t = \phi \frac{v_t - v_{\min}}{v_{\max} - v_{\min}} - \kappa \text{collision}_t, \quad (26)$$

where v_t , v_{\min} , and v_{\max} are the current speed, minimum speed, and maximum speed, respectively. For the first term, it encourages the vehicle to keep high speed to learn to avoid the car in front and gives a reward weight ϕ . Collision is a binary variable that indicates whether a collision occurs between the controlled vehicle and other vehicles. Once a collision occurs, the mission will be terminated and accumulated a negative reward of κ .

5.3 Comparison algorithms

The algorithms under examination in this study encompass model-free methods including RDQN, Proximal Policy Optimization (PPO), DDPG and SAC. While Model-Based Policy Optimization (MBPO) [13] is compared as well, which represents SOTA in model-based RL. RDQN, a potent baseline, combines multiple effective tricks with DQN. Although RDQN itself has PER, in the experiment we will test PER alone as an ablation condition, so RDQN refers to RDQN without PER by default, otherwise it will be marked as RDQN+PER. PPO, the leading model-free approach for discrete actions, is renowned for its stability. SAC, initially designed for entropy RL, is one of the most advanced off-policy methods that balances exploration and exploitation. MBPO integrates an ensemble model into SAC to simulate the environment and enhance the algorithm’s planning capabilities. To simplify the presentation in the experiments, in the discrete action space environment, CEA is built within the framework of RDQN, while in the continuous action space environment, CEA is built within the framework of DDPG. It is important to note that CEA remains a model-free method, as it learns solely from state transition rules and does not perform planning.

5.4 Parameters and equipments

The algorithms’ parameters are disclosed in the Appendix B. We test the algorithm on the consumer-grade graphics card RTX3060 and the high-speed computing card A100 and found no obvious difference. Finally, we implement all

Table 2: Results of experiments. Indicators include the mean, variance and final convergence value of the entire training curve. The higher the Mean and Final, the better; the lower the Std, the better.

Method	Highway			SUMO			Pendulum			Lunar lander		
	Mean	Std	Final	Mean	Std	Final	Mean	Std	Final	Mean	Std	Final
CEA (ours)	29.6	17.2	51.5	<u>-994.3</u>	1134.7	-185.5	-677.8	459.3	-197.8	<u>-157.1</u>	77.9	-94.3
CEA+PER (ours)	25.7	14.1	<u>41.5</u>	-1090.3	1125.4	<u>-245.4</u>	<u>-615.2</u>	474.9	<u>-172.5</u>	-239.7	80.2	-238.4
MBPO	4.7	2.7	3.7	-2455.2	719.1	-3009.6	-	-	-	-	-	-
RDQN	24.7	14.4	13.5	-1209.5	1111.3	-280.7	-	-	-	-	-	-
SAC	9.8	6.75	9.6	-2603.1	1554.3	-1327.5	-624.6	401.7	-345.7	-212.0	62.5	-239.3
PPO	<u>29.5</u>	9.1	34.4	-875.7	524.7	-389.9	-1151.3	171.3	-992.2	-157.3	89.8	<u>-112.7</u>
DDPG	-	-	-	-	-	-	-516.7	468.9	-146.5	-143.2	105.4	-113.0

Table 3: Ablation experiments on PER and CEA. Backbones of Highway and SUMO is RDQN, and the backbone of the other two is DDPG.

Method	Highway		SUMO		Pendulum		Lunar lander	
	Mean	Final	Mean	Final	Mean	Final	Mean	Final
backbone+CEA (ours)	29.6	51.5	-994.3	-185.5	-667.8	-197.8	<u>-157.1</u>	-94.3
backbone+CEA+PER (ours)	<u>25.7</u>	<u>41.5</u>	-1090.3	-245.4	-615.2	-172.5	-239.7	-238.4
backbone+PER	22.2	9.8	-1209.5	-280.7	-493.8	-152.9	-221.9	-191.0
backbone	24.7	13.5	<u>-1018.4</u>	<u>-234.2</u>	<u>-516.7</u>	<u>-146.5</u>	-143.2	<u>-113.0</u>

experiments on a RTX3060 GPU. However, if the experimental environment is more complex and the amount of data is larger, we believe that this requires better equipments.

6 Experimental results

This section will present results of comparative and ablation experiments. To ensure fairness, all algorithms are trained using multiple seeds to minimize randomness. All seeds will be disclosed in the title of the experiment figures. Different algorithms are marked with different colors and markers. The shaded area of each algorithm represents the maximum and minimum return of each training set in different seeds, while the solid line shows the average value. All curves display exponential moving averages with a smoothing factor of 0.05.

Referring to Fig. 7(a) for the training performance in SUMO, the algorithm proposed in this paper is the curve CEA. In the traffic signal control mission, most algorithms converge to similar optimal levels, differing mainly in convergence speed and control stability. Notably, MBPO fails to converge, as it struggles with generalizing reward predictions, which leads to a poor model and inadequate guidance for the training of RL agent. The visualization of the model training results of MBPO are shown in Subsection 7.1.

Referring to Fig. 7(b) for Highway benchmark. PPO exhibits the quickest convergence speed, but its final performance level falls short compared to CEA. Additionally, RDQN encounters a noticeable catastrophic forgetting issue in the last period training. In Highway, initial environment conditions occasionally lead to vehicles being too close, causing the algorithm to struggle in controlling promptly. This results in frequent collisions and low returns, manifesting as a large shaded area in the figure.

Refer to Fig 7(c), in the pendulum task, CEA performs poorly. The training effect of DDPG with CEA module is not as good as DDPG itself. We think it may be because the environment does not meet the assumption of mutual simulation, or it may be related to insufficient training of STA.

The experimental results of the Lunar lander task refer to Fig. 7(d), CEA still maintains a good performance, indicating that it can still play a role in the continuous action space. Combining the results of pendulum and lunar lander, we believe that we need to further consider how to define the soft bisimulation assumption and consider further improvements to CEA.

We present experimental result in Table 2. The boldface indicates the best performance, and the underlined indicates the second-best performance. It can be observed that CEA has an excellent overall performance. The second is DDPG, but DDPG cannot support discrete action space tasks well.

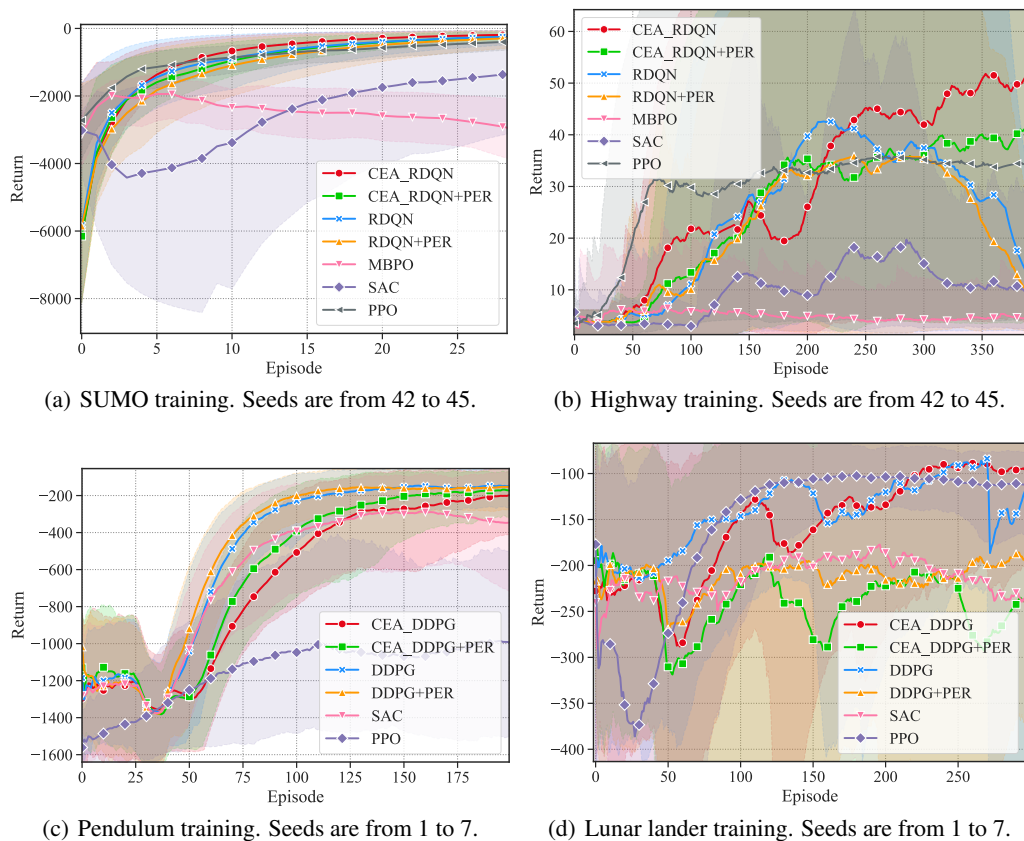


Figure 7: Training process of all experimental environments

The ablation experiments are shown in Table 3, which mainly focus on backbone, CEA and PER. It is observed that PER does not necessarily play a critical role, but CEA maintains the performance improvement. We believe that when the reward signal is dense, PER may not lead to improvement.

The following section is about innovative study, focusing on the details of the experiments and innovative methods in this paper.

7 Innovation study

In this section, we will critically examine the limitations of MBPO and delve into the specifics of our novel contributions, which consist of the STA and CEA methodologies.

7.1 The deficiency of model-based RL

Here we denote the virtual environmental model used in model-based RL as model. The primary challenge lies in maintaining model accuracy in dynamic environments, where frequent updates are necessary but can compromise prediction precision. Our observations reveal that while models can learn state transitions relatively well in non-stationary settings like traffic but struggle to capture reward signals, which can significantly impair model

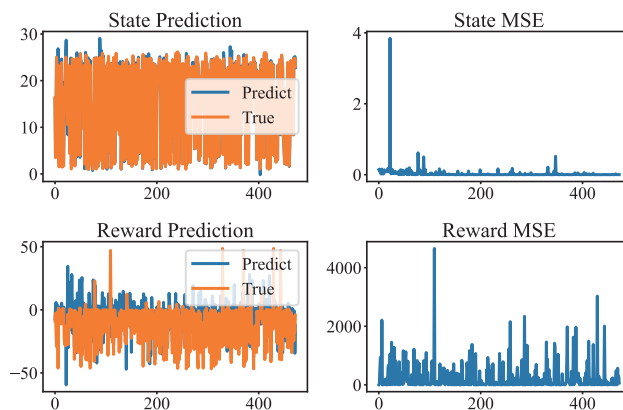


Figure 8: The training of MBPO’s environment model on the SUMO. MBPO is committed to maintaining a virtual environment composed of an integrated neural network model, which accepts the input of the current state and action, and then outputs the prediction and reward value of the next state. It is observed from the figure that the model learns the state transfer law well, but it is difficult to accurately predict the reward value.

training. This issue is illustrated in Fig. 8. Consequently, this motivates the development of STA and CEA.

7.2 Generation of state transition autoencoder

The STA generates state transition vectors based on counterfactual actions. Fig. 10 shows generative matrices for different tasks: initial training on the left and final results on the right, with three representative matrices from each stage. The vertical axis represents counterfactual actions, grouped and ordered, while the horizontal axis shows components of state transition vectors. Each row of colored blocks is a complete vector. As training progresses, the autoencoder better captures state transition dynamics, shown as clusters of dark or light blocks. The randomness of vectors reflects non-stationarity of environments, justifying the use of variational autoencoders.

For experience augmentation as shown in Fig. 9, CEA expands experiences rapidly initially but slows as experience accumulates. Once a threshold is reached, we limit adding counterfactual experience, focusing on real experiences. When the experience pool is full, counterfactual experiences are no longer added. SAC and MBPO have identical experience growth rates, leading to almost overlapping curves in the figure.

Finally, although PER is not always helpful for CEA, it still reveals the similarity of priority distribution between counterfactual experience and real experience, refer to Fig. 11. We show the kernel density distribution of priorities for two different experiences in SUMO and Highway. The two experiences have similar distribution shapes, indicating the rationality of the construction of counterfactual experience.

8 Discussion and future work

Although our method performs well in many scenarios, there are several challenges with the proposed approach.

The complexity of CEA is a significant concern, since we need to perform maximum entropy optimization sampling via Gaussian kernel density estimation. High-dimensional Gaussian kernel density estimation is usually time-consuming. As well as the computational burden of the CTP, which involves comparing large volumes of counterfactual experience with real data. These challenges are especially pronounced in large experience pools, where time efficiency can be compromised.

In addition, it may also be necessary to consider the rate adjustment of introducing counterfactual experiences, because too few real experiences are difficult to train high-quality STA models for prediction, and when real experiences reach a certain amount, the introduction of counterfactual experiences should be reduced. As shown in Fig. 9, we adopted annealing-style experience supplementation, where the amount of supplementation gradually decreases, which can be further designed into an adaptive form.

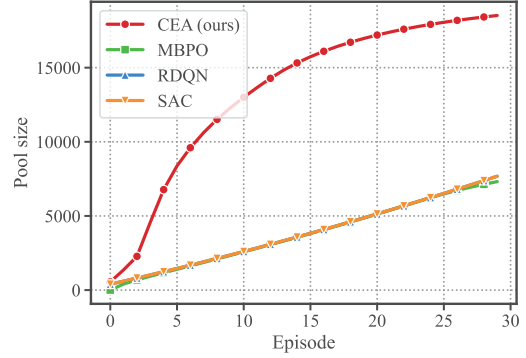


Figure 9: Experience pool size in SUMO mission. It can be observed that through the augmentation of counterfactual experience, the volume of the experience pool rapidly expands, but the rate gradually decreases, and the rate is adjustable.

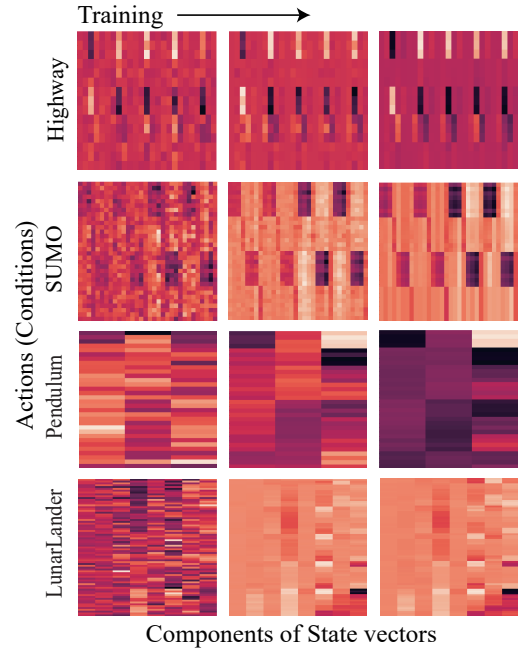
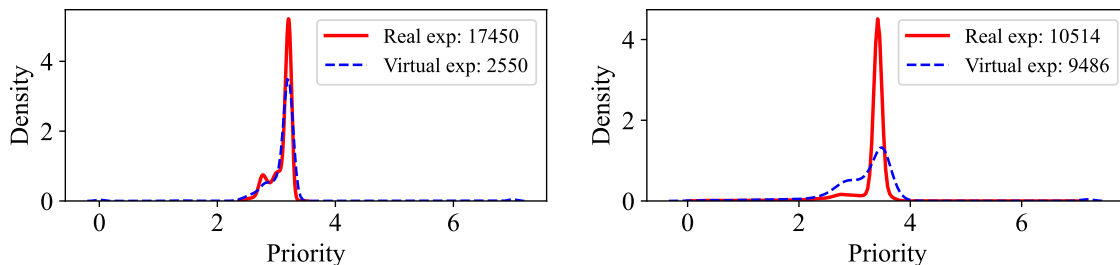


Figure 10: STA generative metrics. From left to right represents the training period. On the vertical axis, we give various actions and put the same actions together. While the transfer vectors generated by the same actions are similar, which should show color blocks. It can be observed that the color blocks are not obvious at the beginning of training, but become more obvious as training progresses, indicating that STA has learned the state transition pattern.



(a) Kernel density estimation of experience features in SUMO. Virtual exp represent counterfactual experience. (b) Kernel density estimation of experience features in High-way. Virtual exp represent counterfactual experience.

Figure 11: Kernel density estimation. The legend gives quantity of the real experience and the counterfactual experience. The horizontal axis represents the priority of PER calculation. The probability density distribution of real experiences and counterfactual experiences, i.e., virtual experiences, can be observed to be aligned in the figure, indicating that the generation quality of counterfactual experiences is relatively high.

9 Conclusion

In this study, we present a comprehensive CEA algorithm, which employs maximum entropy optimization in kernel density estimation to sample counterfactual actions. These actions are then used as generative conditions in the STA to predict subsequent states. STA can be trained effectively using only data from random interactions with the environment, making it easy to train. CEA then uses distance matching to extract suitable reward signals from real-world experiences, resulting in complete counterfactual experiences and storing in the experience pool. We evaluated CEA across various scenarios, where it demonstrated superior overall performance. Our research explores both the practical application and the innovative aspects of STA and CEA, offering valuable insights for future work.

Acknowledgment

This work was supported by Hubei Provincial Key Laboratory of Metallurgical Industry Process System Science (Y202105). This work is also supported by High-Performance Computing Center of Wuhan University of Science and Technology.

Declaration

- **Conflict of Interest** We declare that we have no known competing financial interests or personal relationships that could have appeared to influence the work reported in this paper.
- **Data Availability** The datasets generated during and/or analyzed during the current study are available from the corresponding author on reasonable request.
- **Ethical approval** Our study did not raise any ethical questions, i.e., none of the subjects were humans or living individuals.
- **Informed consent** All authors are aware of this article and agree to its submission.
- **Declaration of generative AI and AI-assisted technologies in the writing process** During the preparation of this work, the first author used generative AI in order to proofread grammar and expression. After using this service, the first author reviewed and edited the content as needed and take full responsibility for the content of the publication.

References

- [1] Michael Laskin, Kimin Lee, Adam Stooke, Lerrel Pinto, Pieter Abbeel, and Aravind Srinivas. Reinforcement learning with augmented data. In *Proceedings of the 34th International Conference on Neural Information Processing Systems*, NIPS '20, Red Hook, NY, USA, 2020. Curran Associates Inc.
- [2] Amy Zhang, Rowan McAllister, Roberto Calandra, Yarín Gal, and Sergey Levine. Learning invariant representations for reinforcement learning without reconstruction, 2021.

- [3] Roberta Raileanu, Max Goldstein, Denis Yarats, Ilya Kostrikov, and Rob Fergus. Automatic data augmentation for generalization in deep reinforcement learning, 2021.
- [4] Denis Yarats, Ilya Kostrikov, and Rob Fergus. Image augmentation is all you need: Regularizing deep reinforcement learning from pixels. In *International Conference on Learning Representations*, 2021.
- [5] Denis Yarats, Rob Fergus, Alessandro Lazaric, and Lerrel Pinto. Mastering visual continuous control: Improved data-augmented reinforcement learning, 2021.
- [6] Nicklas Hansen and Xiaolong Wang. Generalization in reinforcement learning by soft data augmentation. In *2021 IEEE International Conference on Robotics and Automation (ICRA)*, pages 13611–13617, 2021.
- [7] Yuewen Sun, Erli Wang, Biwei Huang, Chaochao Lu, Lu Feng, Changyin Sun, and Kun Zhang. Acamda: Improving data efficiency in reinforcement learning through guided counterfactual data augmentation. *Proceedings of the AAAI Conference on Artificial Intelligence*, 38(14):15193–15201, Mar. 2024.
- [8] Danijar Hafner, Timothy Lillicrap, Ian Fischer, Ruben Villegas, David Ha, Honglak Lee, and James Davidson. Learning latent dynamics for planning from pixels. In Kamalika Chaudhuri and Ruslan Salakhutdinov, editors, *Proceedings of the 36th International Conference on Machine Learning*, volume 97 of *Proceedings of Machine Learning Research*, pages 2555–2565. PMLR, 09–15 Jun 2019.
- [9] Alex X. Lee, Anusha Nagabandi, Pieter Abbeel, and Sergey Levine. Stochastic latent actor-critic: Deep reinforcement learning with a latent variable model. In H. Larochelle, M. Ranzato, R. Hadsell, M.F. Balcan, and H. Lin, editors, *Advances in Neural Information Processing Systems*, volume 33, pages 741–752. Curran Associates, Inc., 2020.
- [10] Denis Yarats, Amy Zhang, Ilya Kostrikov, Brandon Amos, Joelle Pineau, and Rob Fergus. Improving sample efficiency in model-free reinforcement learning from images. *Proceedings of the AAAI Conference on Artificial Intelligence*, 35(12):10674–10681, May 2021.
- [11] William Harvey, Saeid Naderiparizi, and Frank Wood. Conditional image generation by conditioning variational auto-encoders, 2022.
- [12] Diederik P Kingma and Max Welling. Auto-encoding variational bayes, 2022.
- [13] Michael Janner, Justin Fu, Marvin Zhang, and Sergey Levine. When to trust your model: Model-based policy optimization. In H. Wallach, H. Larochelle, A. Beygelzimer, F. d'Alché-Buc, E. Fox, and R. Garnett, editors, *Advances in Neural Information Processing Systems*, volume 32. Curran Associates, Inc., 2019.
- [14] Judea Pearl. Causal inference. In Isabelle Guyon, Dominik Janzing, and Bernhard Schölkopf, editors, *Proceedings of Workshop on Causality: Objectives and Assessment at NIPS 2008*, volume 6 of *Proceedings of Machine Learning Research*, pages 39–58, Whistler, Canada, 12 Dec 2010. PMLR.
- [15] Christopher J. C. H. Watkins and Peter Dayan. Q-learning. *Machine Learning*, 8(3):279–292, May 1992.
- [16] Volodymyr Mnih, Koray Kavukcuoglu, David Silver, Andrei A. Rusu, Joel Veness, Marc G. Bellemare, Alex Graves, Martin Riedmiller, Andreas K. Fidjeland, Georg Ostrovski, Stig Petersen, Charles Beattie, Amir Sadik, Ioannis Antonoglou, Helen King, Dhharshan Kumaran, Daan Wierstra, Shane Legg, and Demis Hassabis. Human-level control through deep reinforcement learning. *Nature*, 518(7540):529–533, Feb 2015.
- [17] Timothy P. Lillicrap, Jonathan J. Hunt, Alexander Pritzel, Nicolas Heess, Tom Erez, Yuval Tassa, David Silver, and Daan Wierstra. Continuous control with deep reinforcement learning, 2019.
- [18] Tuomas Haarnoja, Aurick Zhou, Kristian Hartikainen, George Tucker, Sehoon Ha, Jie Tan, Vikash Kumar, Henry Zhu, Abhishek Gupta, Pieter Abbeel, and Sergey Levine. Soft actor-critic algorithms and applications, 2019.
- [19] Petros Christodoulou. Soft actor-critic for discrete action settings, 2019.
- [20] Tom Schaul, John Quan, Ioannis Antonoglou, and David Silver. Prioritized experience replay, 2016.
- [21] Jian Sun, Jianxin Zhang, Lei Liu, Yanming Wu, and Qihe Shan. Output consensus control of multi-agent systems with switching networks and incomplete leader measurement. *IEEE Transactions on Automation Science and Engineering*, 21(4):6643–6652, 2024.
- [22] Jian Sun, Hongbo Lei, Jianxin Zhang, Lei Liu, and Qihe Shan. Adaptive consensus control of multiagent systems with an unstable high-dimensional leader and switching topologies. *IEEE Transactions on Industrial Informatics*, 20(9):10946–10953, 2024.
- [23] Chao Yu, Akash Velu, Eugene Vinitzky, Jiaxuan Gao, Yu Wang, Alexandre Bayen, and YI WU. The surprising effectiveness of ppo in cooperative multi-agent games. In S. Koyejo, S. Mohamed, A. Agarwal, D. Belgrave, K. Cho, and A. Oh, editors, *Advances in Neural Information Processing Systems*, volume 35, pages 24611–24624. Curran Associates, Inc., 2022.

- [24] Kurtland Chua, Roberto Calandra, Rowan McAllister, and Sergey Levine. Deep reinforcement learning in a handful of trials using probabilistic dynamics models. In S. Bengio, H. Wallach, H. Larochelle, K. Grauman, N. Cesa-Bianchi, and R. Garnett, editors, *Advances in Neural Information Processing Systems*, volume 31. Curran Associates, Inc., 2018.
- [25] Danijar Hafner, Timothy Lillicrap, Jimmy Ba, and Mohammad Norouzi. Dream to control: Learning behaviors by latent imagination, 2020.
- [26] Shantian Yang, Bo Yang, Zheng Zeng, and Zhongfeng Kang. Causal inference multi-agent reinforcement learning for traffic signal control. *Information Fusion*, 94:243–256, 2023.
- [27] Chaochao Lu, Biwei Huang, Ke Wang, José Miguel Hernández-Lobato, Kun Zhang, and Bernhard Schölkopf. Sample-efficient reinforcement learning via counterfactual-based data augmentation. *CoRR*, abs/2012.09092, 2020.
- [28] Silviu Pitis, Elliot Creager, Ajay Mandlekar, and Animesh Garg. Mocoda: Model-based counterfactual data augmentation. In S. Koyejo, S. Mohamed, A. Agarwal, D. Belgrave, K. Cho, and A. Oh, editors, *Advances in Neural Information Processing Systems*, volume 35, pages 18143–18156. Curran Associates, Inc., 2022.
- [29] Michael Laskin, Aravind Srinivas, and Pieter Abbeel. Curl: Contrastive unsupervised representations for reinforcement learning. In Hal Daumé III and Aarti Singh, editors, *Proceedings of the 37th International Conference on Machine Learning*, volume 119 of *Proceedings of Machine Learning Research*, pages 5639–5650. PMLR, 13–18 Jul 2020.
- [30] Richard S. Sutton. Learning to predict by the methods of temporal differences. *Machine Learning*, 3(1):9–44, Aug 1988.
- [31] Richard S. Sutton, David McAllester, Satinder Singh, and Yishay Mansour. Policy gradient methods for reinforcement learning with function approximation. In *Proceedings of the 12th International Conference on Neural Information Processing Systems, NIPS’99*, page 1057–1063, Cambridge, MA, USA, 1999. MIT Press.
- [32] Richard S Sutton and Andrew G Barto. *Reinforcement learning: An introduction*. MIT press, 2018.
- [33] Lihong Li, Thomas J Walsh, and Michael L Littman. Towards a unified theory of state abstraction for mdps. *AI&M*, 1(2):3, 2006.
- [34] Robert Givan, Thomas Dean, and Matthew Greig. Equivalence notions and model minimization in markov decision processes. *Artificial intelligence*, 147(1-2):163–223, 2003.
- [35] Jonathan Ho and Stefano Ermon. Generative adversarial imitation learning. In *Neural Information Processing Systems*, 2016.
- [36] Faraz Torabi, Garrett Warnell, and Peter Stone. Generative adversarial imitation from observation. In *Imitation, Intent, and Interaction (I3) Workshop at ICML 2019*, Long Beach, California, USA, June 2019.
- [37] Zhendong Wang, J Jonathan Hunt, and Mingyuan Zhou. Diffusion policies as an expressive policy class for offline reinforcement learning. *International Conference on Learning Representations*, 2023.
- [38] Somil Bansal, Roberto Calandra, Kurtland Chua, Sergey Levine, and Claire Tomlin. Mbmf: Model-based priors for model-free reinforcement learning, 2017.
- [39] Jianlin Su. Variational autoencoder (part 1), Mar 2018.
- [40] Mark Towers, Ariel Kwiatkowski, Jordan Terry, John U Balis, Gianluca De Cola, Tristan Deleu, Manuel Goulão, Andreas Kallinteris, Markus Krimmel, Arjun KG, et al. Gymnasium: A standard interface for reinforcement learning environments. *arXiv preprint arXiv:2407.17032*, 2024.
- [41] Lucas N. Alegre, Ana L. C. Bazzan, and Bruno C. da Silva. Quantifying the impact of non-stationarity in reinforcement learning-based traffic signal control. *PeerJ Computer Science*, 7:e575, 2021.
- [42] Sindhu Padakandla, Prabuchandran K. J., and Shalabh Bhatnagar. Reinforcement learning algorithm for non-stationary environments. *Applied Intelligence*, 50(11):3590–3606, June 2020.
- [43] Pablo Alvarez Lopez, Michael Behrisch, Laura Bieker-Walz, Jakob Erdmann, Yun-Pang Flötteröd, Robert Hilbrich, Leonhard Lücken, Johannes Rummel, Peter Wagner, and Evamarie Wießner. Microscopic traffic simulation using sumo. In *The 21st IEEE International Conference on Intelligent Transportation Systems*. IEEE, 2018.
- [44] Lucas N. Alegre. SUMO-RL. <https://github.com/LucasAlegre/sumo-rl>, 2019.
- [45] James Ault and Guni Sharon. Reinforcement learning benchmarks for traffic signal control. In *Proceedings of the Thirty-fifth Conference on Neural Information Processing Systems (NeurIPS 2021) Datasets and Benchmarks Track*, December 2021.

- [46] Jinming Ma and Feng Wu. Feudal multi-agent deep reinforcement learning for traffic signal control. In *Proceedings of the 19th International Conference on Autonomous Agents and MultiAgent Systems*, AAMAS '20, page 816–824, Richland, SC, 2020. International Foundation for Autonomous Agents and Multiagent Systems.
- [47] Edouard Leurent. An environment for autonomous driving decision-making. <https://github.com/eleurent/highway-env>, 2018.
- [48] Wei Zhou, Dong Chen, Jun Yan, Zhaojian Li, Huilin Yin, and Wanchen Ge. Multi-agent reinforcement learning for cooperative lane changing of connected and autonomous vehicles in mixed traffic. *Autonomous Intelligent Systems*, 2(1):5, 2022.
- [49] Hanlin Tian, Kethan Reddy, Yuxiang Feng, Mohammed Qudus, Yiannis Demiris, and Panagiotis Angeloudis. Enhancing autonomous vehicle training with language model integration and critical scenario generation, 2024.

A Calculation of evidence lower bound

Here we provide the calculation process of $\mathbb{D}_{KL} [q(z|d, a)||p(z|a)]$, where $q(z|d, a)$ follows $N(\mu, \sigma)$, where μ and σ depend on the output of encoder. If we input multiple conditions for batch calculation, it should be a multivariate normal distribution, but we can give the calculation for a univariate normal distribution to generalize.

Here we substitute the normal distribution probability density function in $\mathbb{D}_{KL} [q(z|d, a)||p(z|a)]$:

$$\begin{aligned}
& \mathbb{D}_{KL}(N(\mu, \sigma^2)||N(0, 1)) \\
&= \int \frac{1}{\sqrt{2\pi\sigma^2}} e^{-(x-\mu)^2/2\sigma^2} \left(\log \frac{e^{-(x-\mu)^2/2\sigma^2}/\sqrt{2\pi\sigma^2}}{e^{-x^2/2}/\sqrt{2\pi}} \right) dx \\
&= \int \frac{1}{\sqrt{2\pi\sigma^2}} e^{-(x-\mu)^2/2\sigma^2} \log \left\{ \frac{1}{\sqrt{\sigma^2}} \exp \left\{ \frac{1}{2} [x^2 - (x-\mu)^2/\sigma^2] \right\} \right\} dx \\
&= \frac{1}{2} \int \frac{1}{\sqrt{2\pi\sigma^2}} e^{-(x-\mu)^2/2\sigma^2} [-\log \sigma^2 + x^2 - (x-\mu)^2/\sigma^2] dx.
\end{aligned} \tag{1}$$

We take apart the square brackets on the right side of the integral and calculate them separately. The first is:

$$\begin{aligned}
& \int \frac{1}{\sqrt{2\pi\sigma^2}} e^{-(x-\mu)^2/2\sigma^2} [-\log \sigma^2] dx \\
&= [-\log \sigma^2] \int \frac{1}{\sqrt{2\pi\sigma^2}} e^{-(x-\mu)^2/2\sigma^2} dx \\
&= -\log \sigma^2.
\end{aligned} \tag{2}$$

The second is:

$$\begin{aligned}
& \int \frac{x^2}{\sqrt{2\pi\sigma^2}} e^{-(x-\mu)^2/2\sigma^2} dx \\
&= \mathbb{E}_{x \sim N(\mu, \sigma^2)}(x^2) \\
&= \mu^2 + \sigma^2.
\end{aligned} \tag{3}$$

The third is:

$$\begin{aligned}
& \int \frac{1}{\sqrt{2\pi\sigma^2}} e^{-(x-\mu)^2/2\sigma^2} [-(x-\mu)^2/\sigma^2] dx \\
&= -\mathbb{E}_{x \sim N(\mu, \sigma^2)}(x-\mu)^2/\sigma^2 \\
&= -\sigma^2/\sigma^2 \\
&= -1.
\end{aligned} \tag{4}$$

Therefore we give

$$\mathbb{D}_{KL} [q(z|d, a)||p(z|a)] = \frac{1}{2} \sum (-\log \sigma^2 + \mu^2 + \sigma^2 - 1). \tag{5}$$

Table 1: Parameter settings for Rainbow DQN, SAC-discrete, CEA, PPO, DDPG and MBPO algorithms respectively.

Model	Parameter	Value	Description
Rainbow DQN	gamma	0.99	Discount factor for future rewards
	alpha	0.2	Determines how much prioritization is used
	beta	0.6	Determines how much importance sampling is used
	prior_eps	1e-6	Guarantees every transition can be sampled
	v_min	0	Min value of support
	v_max	200	Max value of support
	atom_size	51	The unit number of support
	memory_size	20000	Size of the replay buffer
	batch_size	128	Batch size for updates
	target_update	100	Period for target model's hard update
SAC-discrete	actor_lr	5e-4	Learning rate for the actor network
	critic_lr	5e-3	Learning rate for the critic network
	alpha_lr	1e-3	Learning rate for the temperature parameter
	hidden_dim	128	Dimension of hidden layers
	gamma	0.98	Discount factor for future rewards
	tau	0.005	Soft update parameter
	buffer_size	20000	Size of the replay buffer
	target_entropy	1.36	Target entropy for the policy
	model_alpha	0.01	Weighting factor in the model loss function
	total_epochs	1	Total number of training epochs
	minimal_size	500	Minimum size of the replay buffer before updating
	batch_size	64	Batch size for updates
CEA	memory_size	20000	Size of the replay buffer
	batch_size	128	Batch size for updates
	target_update	100	Period for target model's hard update
	threshold_ratio	0.1	Threshold ratio for choosing CTP
PPO	actor_lr	3e-4	Learning rate for the actor network
	critic_lr	3e-4	Learning rate for the critic network
	gamma	0.99	Discount factor for future rewards
	total_epochs	1	Number of training iterations
	total_episodes	100	Number of games played per training iteration
	eps	0.2	Clipping range parameter for the PPO objective ($1 - \text{eps}$ to $1 + \text{eps}$)
	epochs	10	Number of epochs per training sequence in PPO
MBPO	real_ratio	0.5	Ratio of real to model-generated data
	actor_lr	5e-4	Learning rate for the actor network
	critic_lr	5e-3	Learning rate for the critic network
	alpha_lr	1e-3	Learning rate for the temperature parameter
	hidden_dim	128	Dimension of hidden layers
	gamma	0.98	Discount factor for future rewards
	tau	0.005	Soft update parameter
	buffer_size	20000	Size of the replay buffer
	target_entropy	1.36	Target entropy for the policy
	model_alpha	0.01	Weighting factor in the model loss function
	rollout_batch_size	1000	Batch size for rollouts
	rollout_length	1	Length of the model rollouts
	DDPG	actor_lr	2e-4
critic_lr		2e-4	Learning rate of critic network
hidden_dim		128	Dimension of hidden layers
buffer_size		5e4	Size of replay buffer
minimal_size		5e3	Minimum sample size
gamma		0.98	Discount factor
sigma		0.01	Standard deviation of Gaussian noise
tau		0.005	Soft update parameter
batch_size		128	Batch size for training

B Parameters of all algorithms

Here we provide the parameter settings for all algorithms in the experiment, as shown in Fig. 1. It should be noted that in SAC-discrete parameter settings, `target_entropy` is calculated by $0.98(-\log(1/\text{action_space}))$. The same is true in MBPO. And the RL backbone of MBPO is SAC-discrete.